

Arrested coalescence of multicellular aggregates

David Oriola,^{1,*} Miquel Marin-Riera,¹ Germaine Aalderink,¹ Kerim Anlas,¹ Nicola Gritti,¹ James Sharpe,^{1,2} and Vikas Trivedi^{1,3,†}

¹*EMBL Barcelona, Dr. Aiguader, 88, 08003, Barcelona, Spain*

²*Institució Catalana de Recerca i Estudis Avançats, 08010, Barcelona, Spain*

³*EMBL Heidelberg, Developmental Biology Unit, 69117 Heidelberg, Germany*

Multicellular aggregates are known to exhibit liquid-like properties. The fusion process of two cell aggregates is commonly studied as the coalescence of two viscous drops. However, tissues are complex materials, which usually exhibit viscoelastic behaviour. It is known that elastic effects can prevent the complete fusion of two drops, a phenomenon known as arrested coalescence. Here we report the presence of this phenomenon in aggregates of mouse embryonic stem cells and provide a theoretical framework which agrees with the experiments. In addition, agent-based simulations show that cell protrusion activity controls a solid-to-fluid phase transition, revealing that arrested coalescence can be found in the vicinity of an unjamming transition. By analyzing the dynamics of the fusion process it is possible to infer mechanical parameters of the aggregates, such as the viscoelastic relaxation time and the elastocapillary number. Our work provides a simple *in vitro* method to characterize the mechanical properties of 3D multicellular aggregates and sheds light on the impact of cellular activity on tissue mechanics.

Shaping of organs during morphogenesis results from the material response of the constituent tissues to the forces which in turn are generated by them. Understanding the material properties of biological tissues holds key to elucidate how shape and form emerge during morphogenesis both *in vivo* during embryonic development [1, 2], as well as *in vitro* in the context of synthetic morphogenesis [3–5]. For instance, viscous dissipation allows tissues to gradually change their shape without accumulation of significant stresses [6, 7] and adapt to different environments. Embryonic tissues are known to exhibit liquid-like properties: they round up [8, 9], fuse [10], engulf other tissues [11] and segregate or sort from heterotypic cell mixtures [12, 13]. However, tissues are also known to exhibit elastic behaviour which can critically affect the final tissue configuration [8, 9, 14]. Unlike viscous forces, which only affect the rate of deformation of the tissue, elastic forces can resist deformation leading to a non-trivial final tissue configuration. Indeed jamming [14] and viscoelastic [8, 15] effects have been shown to be critical in different morphogenetic processes.

The mechanical properties of tissues have been measured using a wide range of techniques (for a detailed review see Refs. [16, 17]). Absolute measurements of the tissue surface tension and the material properties of tissues are possible by using microplates [8, 18, 19], axisymmetric drop shape analysis [9, 20], micropipette aspiration [21] and drop sensors [22, 23]. In all cases, an external force is used to probe the system. A few methods have been used to obtain relative measurements at the tissue scale: laser ablation [24] and the fusion of tissue aggregates [25–27]. In both cases the measured velocities can be related to material properties. In the first case, the strain rate is related to ratio of tissue stress and viscosity [24], while in the second case the

speed of fusion is dictated by the viscocapillary velocity, which is the ratio between tissue surface tension and viscosity [26, 28–31]. Of all the previous methods, limited appreciation has been given to the fusion method [27, 32], which is arguably one of the simplest methods to obtain relative measures. Additional advantages of the method are the fact that there is no need of a calibrated probe and it is a non-contact method [16]. The fusion of viscoelastic droplets is known to exhibit a phenomenon known as arrested coalescence [33–35], whereby the degree of coalescence is related to the elasticity of the material. The stable anisotropic shapes it can produce, have been exploited extensively to produce emulsions in a wide range of industries like food, cosmetics, petroleum and pharmaceutical formulations [33–37]. Despite the fact that the sintering of viscous droplets is a well known problem [26, 28–31, 38, 39], a mathematical formulation akin to the one of Frenkel and Eshelby [28, 40] for the case of two coalescing viscoelastic solid drops is, to our knowledge, still missing. Furthermore, this phenomenon has received only limited appreciation in the context of tissue engineering [41].

In this work, we report the observation of arrested coalescence in mouse embryonic stem cell aggregates and show that a minimal Kelvin-Voigt model successfully captures the dynamics of the process. By fitting our model to the experiments, the viscoelastic relaxation time τ_v and the elastocapillary number Ec can be obtained. Finally, by using agent-based simulations of the fusion process, we show how active cell protrusions drive a solid-to-fluid phase transition and how the supracellular mechanical properties arise from the cell level interactions.

Experimental results. Mouse embryonic stem cells (E14 stem cells) were cultured in Dulbecco's Modified Eagle Medium (DMEM)-based ES-LIF medium and ~ 300 cells/well were aggregated in 96-well U-bottom microplates (Greiner Cellstar, #650970) in $40 \mu\text{L}$ NDiff227[®] (Takara Bio, #Y40002) media for 24h (Fig. 1A). Fusion experiments were carried out by placing two mouse embryonic aggregates in contact with each other (Fig. 1B). The multicellular aggregates were imaged in brightfield mode every 10 min for 10h in a high-content screening PerkinElmer Opera Phenix[®] system. In Fig. 1C an example of the fusion of two cellular aggregates is shown. Arrested coalescence started ~ 3 h after fusion (Fig. 1C and Movie S1), with anisotropic shapes maintained for the next ~ 7 h. Image analysis was done for each aggregate using a custom machine learning-based pipeline (see Supplementary Material). This allowed us to obtain the time evolution of the fusion angle θ (see Figs. 1D and 2A). During the fusion process, the aggregates increased in size due to cell proliferation. To quantify the change in radius we imaged the growth of single aggregates. The average initial radius was $R_0 = 96.7 \pm 0.6 \mu\text{m}$ ($n = 10$, see Supplementary Material) and it increased linearly over time (see Fig. 1E). After the fusion process (~ 4 h) the radius of the aggregates increased by $\simeq 5\%$, corresponding to a $\simeq 15\%$ increase in volume. The doubling time of cells was estimated by simply fitting a linear function to the time evolution of the aggregate radius (see Supplementary Material) and was found to be $T = 13.8 \pm 0.4 \text{ h}$ ($n = 10$, mean \pm SD). Given that the fusion process is ~ 3 times faster than cell division, we conclude that the volume of the cell aggregates does not significantly change during the fusion process.

Continuum model. In order to understand the fusion dynamics, we considered each multicellular aggregate as a drop of an homogeneous incompressible Kelvin-Voigt material with effective shear viscosity η , elastic modulus E and surface tension γ . This simple constitutive model has been shown to be successful in describing the mechanical properties of multiple types of tissue explants [9] and it is arguably the simplest model to describe arrested coalescence [35]. The constitutive equation for the stress tensor $\boldsymbol{\sigma}$ reads $\boldsymbol{\sigma} = 2\eta\dot{\boldsymbol{\epsilon}} + E\boldsymbol{\epsilon} - P\mathbb{I}$, where $\boldsymbol{\epsilon} = \frac{1}{2}[\nabla\mathbf{u} + (\nabla\mathbf{u})^T]$ is the symmetric strain tensor, P is the hydrostatic pressure and \mathbf{u} is the displacement field. Given that cell proliferation is negligible on the timescale of fusion, we approximate the continuity equation as $\nabla \cdot \dot{\mathbf{u}} = 0$. Force balance in the bulk and on the surface read $\nabla \cdot \boldsymbol{\sigma} = 0$ and $\boldsymbol{\sigma} \cdot \mathbf{n} = 2\gamma H\mathbf{n}$, respectively, where H is the local mean curvature of the surface and \mathbf{n} is the unit normal vector to the surface. Next, following the work in Refs. [28–31], we approximate the assembly as two identical spherical caps of radius $R(\theta)$ with circular contact ‘neck’ region of radius $r(\theta) = R(\theta) \sin \theta$,

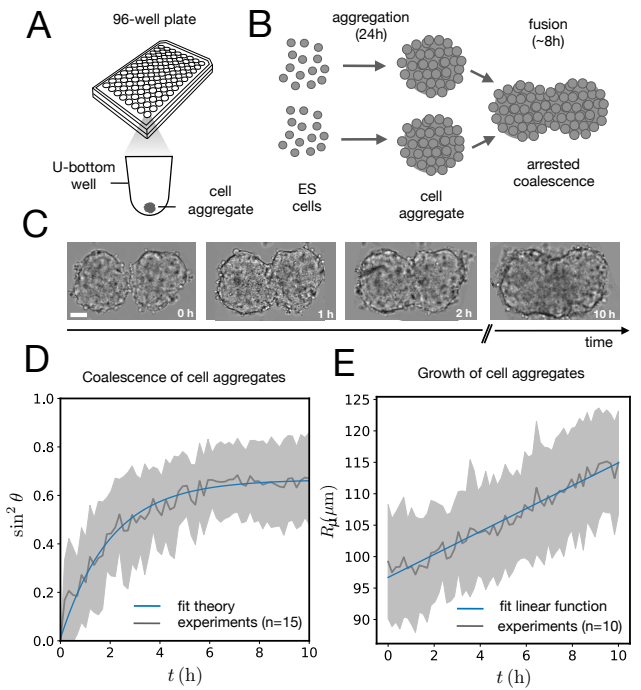


FIG. 1. Arrested coalescence of embryonic stem cell aggregates. A) Spheroids were formed by aggregating mouse embryonic stem cells in low adhesion U-bottom multiwell microplates. B) Cell aggregates were placed in close contact at 24h after aggregation and the fusion process was imaged using a high content microscopy system. C) Bright field images of a fusion event showing the resulting anisotropic shape of the assembly. Notice that the anisotropic shape of the assembly does not change significantly from ~ 2 h to 10h. D) Fusion dynamics quantification showing the averaged time evolution of $\sin^2 \theta$, where θ is the fusion angle of the assembly (see Fig. 2). E) Average radius of a single aggregate over time. Scale bar: $50 \mu\text{m}$.

with fusion angle θ (see Fig. 2A). The dependence of the radius R on θ is determined by the incompressibility condition (see Supplementary Material). The dynamics of the fusion process will be described by the evolution of $\theta(t)$. Let us assume the axis of fusion as \mathbf{e}_x (see Fig. 2A). The end-to-end length $L(\theta)$ of the fusion assembly along this axis will be given by $L(\theta) = 2R(\theta)(1 + \cos \theta)$. It is known that coalescence of viscoelastic solid drops can be suppressed for sufficiently large values of the elastic modulus [35]. The physics at the onset of fusion is not captured by our hydrodynamic model and has its origin on the cell-cell interactions between the two aggregates. To account for such effect we incorporate a pre-strain to the assembly by considering a shift on the rest length $L'(0) = L(0) + \delta L$, being $\delta L/L(0) \ll 1$. The strain is approximated as $\partial_x u \simeq -\varepsilon(\theta)$, with $\varepsilon(\theta) = [L'(0) - L(\theta)]/L'(0) \simeq \varepsilon_P + \varepsilon_L(\theta)$, where $\varepsilon_P = \delta L/L'(0)$ is a pre-strain and $\varepsilon_L(\theta) = 1 - \frac{R(\theta)}{2R_0}(1 + \cos \theta)$ is the strain caused by fusion [35]. The corresponding strain

rate reads $\partial_x \dot{u} \simeq -\dot{\varepsilon}(\theta) = \frac{1}{2R_0} \frac{d}{dt} [R(\theta)(1 + \cos \theta)]$. The previous expression differs from the one used in Refs. [26, 28–31], where strain is defined using the distance between the center of a droplet in the assembly and the fusion plane (i.e. $R(\theta) \cos \theta$), as opposed to the end-to-end length $L(\theta)$. Both expressions are only equivalent for small angles (i.e. $\theta \ll 1$). We will use the end-to-end distance definition to be consistent with previous studies on arrested coalescence [35], where the maximum strain for complete coalescence reads $\varepsilon_L(\pi/2) = 1 - 2^{-2/3} \simeq 0.37$. Using the previous expressions we can calculate the dynamics of θ by equating the work per unit time done by the bulk and surface forces [31] (see Supplementary Material). The equation for the dynamics of the fusion angle $\theta(t)$ reads:

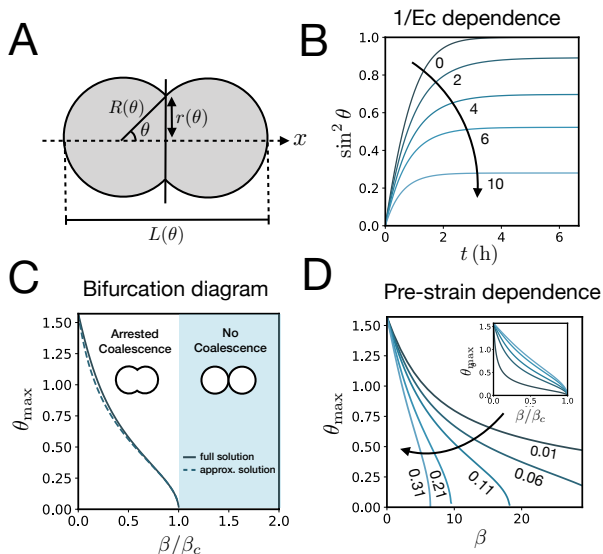


FIG. 2. A) Schematics of two identical droplets fusing along the \mathbf{e}_x axis. θ is the angle of fusion which is $\pi/2$ for complete coalescence and takes a value in the range $(0, \pi/2)$ for arrested coalescence. $R(\theta)$ is the radius of each aggregate, $r(\theta)$ is the neck radius during the fusion process and $L(\theta)$ is the end-to-end length. B) Time evolution of $(r/R)^2 = \sin^2 \theta$ as a function of the inverse elastocapillary number β for $\tau = 4$ h and $\varepsilon_P = 0.11$ by solving Eq. 1. C) Bifurcation diagram showing the steady state coalescence angle θ_{\max} as a function of β/β_c . For $\beta < \beta_c$ the system undergoes a pitchfork bifurcation where the non-fused state loses stability in favour of the fused state. The numerical steady state solution of Eq. 1 is shown as a solid line while the approximate analytical solution assuming $R(\theta) \approx R_0$ is shown as a dashed line (see Supplementary Material). $\varepsilon_P = 0.11$. D) Pre-strain dependence of θ_{\max} on β . Inset: Same plot but rescaling β by its critical value β_c .

$$\dot{\theta} = \frac{2 \cot \theta}{\tau} \left(\frac{R_0}{R(\theta)} \right)^3 [f(\theta) - \beta g(\theta)] \quad (1)$$

where $\tau = \eta R_0 / \gamma$ is the characteristic viscocapillary time, $\text{Ec} \equiv \beta^{-1} = \gamma / (E R_0)$ is the elastocapillary number

[42] and $f(\theta), g(\theta)$ are functions that depend on the angle θ (see Supplementary Material). The elastocapillary number can also be expressed as the ratio of the two main timescales in the system $\text{Ec} = \tau_v / \tau$ where $\tau_v = \eta / E$ is the viscoelastic relaxation timescale. For small angles and $\text{Ec} \rightarrow \infty$, Eq. 1 reduces to the typical form for the sintering of viscous drops [30, 31]. Considering the inverse elastocapillary number β as our bifurcation parameter, we find that for $\beta > \beta_c = 2/\varepsilon_P$, elasticity overcomes surface tension and the stable state is $\theta = 0$, i.e. no fusion (see Supplementary Material). However, for $\beta < \beta_c$, the system undergoes a pitchfork bifurcation whereby the state $\theta = 0$ becomes unstable and droplets fuse (see Fig. 2,B,C). This critical condition $\beta = \beta_c$ is equivalent to $\sigma_P = \frac{2\gamma_c}{R_0}$, which means that coalescence starts when the Laplace pressure equals a pre-stress $\sigma_P = E\varepsilon_P$. Finally, in Fig. 2D we show the dependence of the maximum fusion angle θ_{\max} on the pre-strain ε_P , which significantly varies for large pre-strains. To fit our model to the experimental data, for simplicity we assumed $\varepsilon_P = 0$. The curves were averaged over 15 aggregate fusion events and the resulting curve was numerically fitted to the solution of Eq. 1 (see Fig. 1D). The fitted values read $\beta = 6.7 \pm 0.2$ ($\text{Ec} = 0.149 \pm 0.004$) and $\tau = 12.5 \pm 0.5$ h, giving a viscoelastic relaxation time $\tau_v = 1.9 \pm 0.1$ h (mean \pm SD, $n = 15$). Considering an elastic modulus of embryonic tissues of $E \sim 100$ Pa [19] and $R_0 \simeq 100 \mu\text{m}$, we obtain $\gamma \sim 1$ mN/m and $\eta \sim 10^5$ Pa-s, which compares well with the typical values obtained in parallel plate compression or micropipette aspiration experiments [19, 21].

Agent-based simulations. Despite the Kelvin-Voigt model providing a good fit to the experimental data, the rheology of cell aggregates is indeed much more complicated and it is unclear how cell-cell interactions give rise to the effective macroscopic mechanical properties observed. To understand this, we turned to agent-based simulations of cellular aggregates using the GPU-based software ya||a (see Fig. 3A), which supports easy implementation of diverse cellular behaviours [43]. For simplicity, we considered a minimal model taking into account adherent and contractile protrusion interactions between cells. The dynamics of a cell i with center at \mathbf{x}_i reads:

$$\lambda(\dot{\mathbf{x}}_i - \langle \dot{\mathbf{x}}_j \rangle_i) = \sum_j (\mathbf{F}_{ij}^s + \mathbf{F}_{ij}^a) \quad (2)$$

where $\langle \dot{\mathbf{x}}_j \rangle_i$ is the average velocity of the neighbouring j cells of cell i , \mathbf{F}_{ij}^s is a passive cell-cell interaction force and \mathbf{F}_{ij}^a is an active force to model contractile cell protrusions, which are known to be important in convergence-extension and cell sorting processes [44, 45]. Friction forces are considered to be proportional to the relative velocity of neighbouring cells with friction coefficient λ , a typical assumption used in foam and colloidal systems [46, 47] as well as in tissues [48, 49].

Cells have radius r_0 and the distance between a pair of cells i and j is denoted as $\mathbf{r}_{ij} = \mathbf{x}_i - \mathbf{x}_j$. The passive cell-cell interaction force has a repulsion harmonic force $\mathbf{F}_{ij}^s = K_r(2r_0 - |\mathbf{r}_{ij}|)\hat{\mathbf{r}}_{ij}$ for $|\mathbf{r}_{ij}| < 2r_0$ and a truncated harmonic attractive force such that $\mathbf{F}_{ij}^s = K_{\text{adh}}(2r_0 - |\mathbf{r}_{ij}|)\Theta(r_{\text{max}} - |\mathbf{r}_{ij}|)\hat{\mathbf{r}}_{ij}$ for $|\mathbf{r}_{ij}| > 2r_0$, where $\hat{\mathbf{r}}_{ij} = \mathbf{r}_{ij}/|\mathbf{r}_{ij}|$. The first term describes excluded volume interactions between cells while the last one describes cell-cell adhesion. The active part \mathbf{F}_{ij}^a consists of cells randomly selecting a nearest neighbour and applying a constant force $\mathbf{F}_{ij}^a = -F_p\hat{\mathbf{r}}_{ij}$ if $|\mathbf{r}_{ij}| > 2r_0$, where $F_p > 0$ is defined as contractile (see Supplementary Material). The choice of a constant protrusion force is a simplification of more complicated velocity-force relationships found experimentally [50]. We associate a lifetime to each protrusion τ_{on} and analogously, a waiting time τ_{off} . Thus a protrusion duty ratio can be defined as $\alpha = \tau_{\text{on}}/(\tau_{\text{on}} + \tau_{\text{off}})$. The previous protrusion dynamics is similar to a shot noise process of active origin [51]. Hence, protrusion interactions introduce force dipoles stochastically in the cell aggregate, which are known to induce cell-cell rearrangements and fluidize tissues [52–54].

We analyzed the fusion dynamics in the simulations by using the end-to-end length of the assembly as in the experiments and varied the protrusion force F_p and the duty ratio α (see Fig. 3). We fitted Eq. 1 to the averaged dynamics (Fig. 3B) and extracted the effective macroscopic parameters τ and β . The study revealed the presence of three main regimes according to the inverse elastocapillary number β (see Movies S2-S4): (i) no coalescence ($\beta \gtrsim 50$), (ii) arrested coalescence ($50 \gtrsim \beta \gtrsim 2$) and (iii) complete coalescence ($\beta \lesssim 2$) (Fig. 3C), which qualitatively agree with the regimes found in the continuum model (see Fig. 2). The same regimes are also identified when studying the characteristic viscopillary time τ (see Fig. S1). These results suggest the system undergoes a solid-to-fluid transition for increasing protrusion strength or duty ratio. To assess if the observed transition is similar to a rigidity or a jamming transition, we studied the relative mean squared displacement of cells (Fig. 3D). We found that in regimes (i) and (ii) the behaviour was subdiffusive while the behaviour was mainly diffusive in regime (iii). In addition, we observed that the viscoelastic relaxation time τ_v showed a clear peak at the transition point (see Fig. 3D, inset). Finally, by performing compression/relaxation cycles in parallel plate compression simulations on the aggregates (see Movies S5, S6) we identified the presence of a yield stress in regime (ii), below which the deformation was not recovered during the relaxation process, indicating a plastic behaviour of the material [55]. Hence, we conclude that in our system, arrested coalescence is found at the vicinity of a solid-to-fluid transition, similar to jammed systems [35].

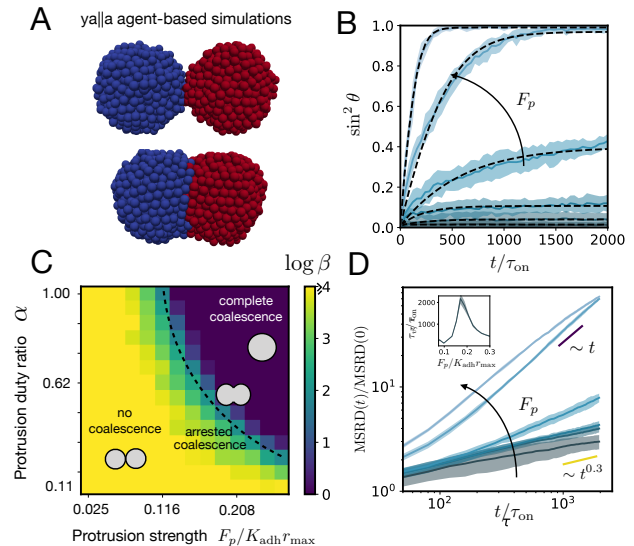


FIG. 3. A) ya|a agent-based simulations of the fusion of two cell aggregates for $F_p/K_{\text{adh}}r_{\text{max}} = 0.125$ and $\alpha = 1$. B) Averaged time evolution of $\sin^2 \theta$ over time ($n = 10$) in the simulations for different cell protrusion strengths $F_p/K_{\text{adh}}r_{\text{max}} = (0.025, 0.061, 0.098, 0.134, 0.171, 0.208)$. $K_{\text{adh}}/K_r = 1$, $r_0/r_{\text{max}} = 0.4$, $\lambda/K_{\text{adh}}\tau_{\text{on}} = 1$, $\alpha = 0.234$, and 1000 cells per aggregate. The numerical fits are done using Eq. 1. C) Colormap of $\log \beta$ in parameter space. Three distinct regions can be identified corresponding to no coalescence, arrested coalescence and complete coalescence. D) Mean squared relative displacement of cells as a function of time for different protrusion strengths $F_p/K_{\text{adh}}r_{\text{max}}$ (same values as in panel B). Cells change from a subdiffusive ($\sim t^{0.3}$) to a diffusive ($\sim t$) behaviour for increasing F_p . Inset. Viscoelastic relaxation time vs protrusion strength.

Discussion. Here we report the phenomenon of arrested coalescence in mouse embryonic cell aggregates and present a viscoelastic theory of sintering to understand the dynamics of the process. We show that a minimal agent-based model considering cell-cell adhesion and dipolar contractile protrusions reproduces arrested coalescence. Additionally, we find that cell protrusion activity controls a solid-to-fluid transition. By combining simulations and continuum theory, we are able to study the dependence of different hydrodynamic quantities on cell-cell interactions. The role of cell protrusions is twofold: on the one hand, it leads to a fluidization process (Fig. 3D) and, on the other hand, it creates an effective surface tension γ that drives the coalescence of the cell aggregates. Although the solid-to-fluid transition is of active origin, it is different from other transitions observed in models of self-propelled particles [56, 57] since the protrusion interactions only introduce dipolar forces. The transition we find resembles recent rigidity transitions driven by active tension fluctuations at cell-cell contacts [58]. Finally, an intrinsic limitation

of our particle-based simulations is the absence of cell shape changes which are known to be critical in tissue rheology [58–61]. Further work should be done to incorporate such effects for example by means of 3D vertex models [62].

Continuum descriptions of drop coalescence have been mainly limited to purely viscous drops [28–31]. This has limited the use of such theories to the determination of viscosity and surface tension, despite tissue stiffness and viscoelastic effects having important implications for tissue engineering and being known to play a major role in cancer [63, 64]. By combining the present method with AFM or microplate experiments, it is possible to obtain a fast, inexpensive full mechanical characterisation of 3D tissue aggregates. We envision that future work on the theory of sintering for viscoelastic materials will be important in the formation of biological structures *in vitro* using bioink units [65].

Acknowledgements. This work was conceived during the COVID-19 pandemic lockdown. We would like to thank all the healthcare professionals who fought against the disease. All authors were supported by the European Molecular Biology Laboratory (EMBL) Barcelona. We also thank M. Merkel, J. Casademunt, X. Diego and all the members of the Trivedi group for illuminating discussions. D.O. acknowledges funding from Juan de la Cierva Incorporación with Project no. IJC2018-035298-I, from the Spanish Ministry of Science, Innovation and Universities (MCIU/AEI).

* david.oriola@embl.es

† trivedi@embl.es

- [1] C.-P. Heisenberg and Y. Bellaïche, “Forces in tissue morphogenesis and patterning,” *Cell*, vol. 153, no. 5, pp. 948–962, 2013.
- [2] H. Hamada, “Role of physical forces in embryonic development,” in *Seminars in cell & developmental biology*, vol. 47, pp. 88–91, Elsevier, 2015.
- [3] B. P. Teague, P. Guye, and R. Weiss, “Synthetic morphogenesis,” *Cold Spring Harbor perspectives in biology*, vol. 8, no. 9, p. a023929, 2016.
- [4] N. Gritti, D. Oriola, and V. Trivedi, “Rethinking embryology in vitro: A synergy between engineering, data science and theory,” *Developmental biology*, 2020.
- [5] E. Garreta, R. D. Kamm, S. M. C. de Sousa Lopes, M. A. Lancaster, R. Weiss, X. Trepant, I. Hyun, and N. Montserat, “Rethinking organoid technology through bioengineering,” *Nature Materials*, pp. 1–11, 2020.
- [6] T. Wyatt, B. Baum, and G. Charras, “A question of time: tissue adaptation to mechanical forces,” *Current opinion in cell biology*, vol. 38, pp. 68–73, 2016.
- [7] R. Clément, B. Dehapiot, C. Collinet, T. Lecuit, and P.-F. Lenne, “Viscoelastic dissipation stabilizes cell shape changes during tissue morphogenesis,” *Current biology*, vol. 27, no. 20, pp. 3132–3142, 2017.
- [8] E.-M. Schötz, R. D. Burdine, F. Jülicher, M. S. Steinberg, C.-P. Heisenberg, and R. A. Foty, “Quantitative differences in tissue surface tension influence zebrafish germ layer positioning,” *HFSP journal*, vol. 2, no. 1, pp. 42–56, 2008.
- [9] M. Yu, A. Mahtabfar, P. Beelen, Y. Demiryurek, D. I. Shreiber, J. D. Zahn, R. A. Foty, L. Liu, and H. Lin, “Coherent timescales and mechanical structure of multicellular aggregates,” *Biophysical journal*, vol. 114, no. 11, pp. 2703–2716, 2018.
- [10] R. Gordon, N. S. Goel, M. S. Steinberg, and L. L. Wiseman, “A rheological mechanism sufficient to explain the kinetics of cell sorting,” *Journal of theoretical biology*, vol. 37, no. 1, pp. 43–73, 1972.
- [11] M. S. Steinberg and M. Takeichi, “Experimental specification of cell sorting, tissue spreading, and specific spatial patterning by quantitative differences in cadherin expression,” *Proceedings of the National Academy of Sciences*, vol. 91, no. 1, pp. 206–209, 1994.
- [12] K. Heintzelman, H. Phillips, and G. Davis, “Liquid-tissue behavior and differential cohesiveness during chick limb budding,” *Development*, vol. 47, no. 1, pp. 1–15, 1978.
- [13] R. A. Foty, G. Forgacs, C. M. Pflieger, and M. S. Steinberg, “Liquid properties of embryonic tissues: Measurement of interfacial tensions,” *Physical review letters*, vol. 72, no. 14, p. 2298, 1994.
- [14] A. Mongera, P. Rowghanian, H. J. Gustafson, E. Shelton, D. A. Kealhofer, E. K. Carn, F. Serwane, A. A. Lucio, J. Giammona, and O. Campàs, “A fluid-to-solid jamming transition underlies vertebrate body axis elongation,” *Nature*, vol. 561, no. 7723, pp. 401–405, 2018.
- [15] O. Luu, R. David, H. Ninomiya, and R. Winklbauer, “Large-scale mechanical properties of xenopus embryonic epithelium,” *Proceedings of the National Academy of Sciences*, vol. 108, no. 10, pp. 4000–4005, 2011.
- [16] K. Sugimura, P.-F. Lenne, and F. Graner, “Measuring forces and stresses in situ in living tissues,” *Development*, vol. 143, no. 2, pp. 186–196, 2016.
- [17] O. Campàs, “A toolbox to explore the mechanics of living embryonic tissues,” in *Seminars in cell & developmental biology*, vol. 55, pp. 119–130, Elsevier, 2016.
- [18] R. A. Foty, C. M. Pflieger, G. Forgacs, and M. S. Steinberg, “Surface tensions of embryonic tissues predict their mutual envelopment behavior,” *Development*, vol. 122, no. 5, pp. 1611–1620, 1996.
- [19] G. Forgacs, R. A. Foty, Y. Shafrir, and M. S. Steinberg, “Viscoelastic properties of living embryonic tissues: a quantitative study,” *Biophysical journal*, vol. 74, no. 5, pp. 2227–2234, 1998.
- [20] R. David, H. Ninomiya, R. Winklbauer, and A. W. Neumann, “Tissue surface tension measurement by rigorous axisymmetric drop shape analysis,” *Colloids and Surfaces B: Biointerfaces*, vol. 72, no. 2, pp. 236–240, 2009.
- [21] K. Guevorkian, M.-J. Colbert, M. Durth, S. Dufour, and F. Brochard-Wyart, “Aspiration of biological viscoelastic drops,” *Physical review letters*, vol. 104, no. 21, p. 218101, 2010.
- [22] O. Campàs, T. Mammoto, S. Hasso, R. A. Sperling, D. O’connell, A. G. Bischof, R. Maas, D. A. Weitz, L. Mahadevan, and D. E. Ingber, “Quantifying cell-generated mechanical forces within living embryonic tissues,” *Nature methods*, vol. 11, no. 2, p. 183, 2014.
- [23] F. Serwane, A. Mongera, P. Rowghanian, D. A. Keal-

- hofer, A. A. Lucio, Z. M. Hockenbery, and O. Campas, "In vivo quantification of spatially varying mechanical properties in developing tissues," *Nature methods*, vol. 14, no. 2, p. 181, 2017.
- [24] I. Bonnet, P. Marcq, F. Bosveld, L. Fetler, Y. Bellaïche, and F. Graner, "Mechanical state, material properties and continuous description of an epithelial tissue," *Journal of The Royal Society Interface*, vol. 9, no. 75, pp. 2614–2623, 2012.
- [25] K. Jakab, B. Damon, F. Marga, O. Doaga, V. Mironov, I. Kosztin, R. Markwald, and G. Forgacs, "Relating cell and tissue mechanics: implications and applications," *Developmental dynamics: an official publication of the American Association of Anatomists*, vol. 237, no. 9, pp. 2438–2449, 2008.
- [26] G. Dechristé, J. Fehrenbach, E. Grisetti, V. Lobjois, and C. Poinard, "Viscoelastic modeling of the fusion of multicellular tumor spheroids in growth phase," *Journal of theoretical biology*, vol. 454, pp. 102–109, 2018.
- [27] R. David, O. Luu, E. W. Damm, J. W. Wen, M. Nagel, and R. Winklbauer, "Tissue cohesion and the mechanics of cell rearrangement," *Development*, vol. 141, no. 19, pp. 3672–3682, 2014.
- [28] J. Frenkel, "Viscous flow of crystalline bodies under the action of surface tension," *J. phys.*, vol. 9, p. 385, 1945.
- [29] O. Pokluda, C. T. Bellehumeur, and J. Vlachopoulos, "Modification of frenkel's model for sintering," *AIChE journal*, vol. 43, no. 12, pp. 3253–3256, 1997.
- [30] M. K. Bellehumeur, Céline T. and J. Vlachopoulos, "The role of viscoelasticity in polymer sintering," *Rheologica acta*, vol. 37, no. 3, pp. 270–278, 1998.
- [31] E. Flenner, L. Janosi, B. Barz, A. Neagu, G. Forgacs, and I. Kosztin, "Kinetic monte carlo and cellular particle dynamics simulations of multicellular systems," *Physical Review E*, vol. 85, no. 3, p. 031907, 2012.
- [32] T. V. Stirbat, A. Mgharbel, S. Bodenec, K. Ferri, H. C. Mertani, J.-P. Rieu, and H. Delanoë-Ayari, "Fine tuning of tissues' viscosity and surface tension through contractility suggests a new role for α -catenin," *PLoS One*, vol. 8, no. 2, 2013.
- [33] P. Dahiya, M. Caggioni, and P. T. Spicer, "Arrested coalescence of viscoelastic droplets: polydisperse doublets," *Philosophical Transactions of the Royal Society A: Mathematical, Physical and Engineering Sciences*, vol. 374, no. 2072, p. 20150132, 2016.
- [34] P. Dahiya, "Arrested coalescence in food emulsions," 2017.
- [35] A. B. Pawar, M. Caggioni, R. W. Hartel, and P. T. Spicer, "Arrested coalescence of viscoelastic droplets with internal microstructure," *Faraday discussions*, vol. 158, no. 1, pp. 341–350, 2012.
- [36] V. Muguet, M. Seiller, G. Barratt, O. Ozer, J. Marty, and J. Grossiord, "Formulation of shear rate sensitive multiple emulsions," *Journal of controlled release*, vol. 70, no. 1-2, pp. 37–49, 2001.
- [37] R. S. Garabedian and J. J. Helble, "A model for the viscous coalescence of amorphous particles," *Journal of colloid and interface science*, vol. 234, no. 2, pp. 248–260, 2001.
- [38] S. Aid, A. Eddhahak, Z. Ortega, D. Froelich, and A. Tcharkhtchi, "Predictive coalescence modeling of particles from different polymers: application to pvdf and pmma pair," *Journal of Materials Science*, vol. 52, no. 19, pp. 11725–11736, 2017.
- [39] D. D. Joseph, *Fluid dynamics of viscoelastic liquids*, vol. 84. Springer Science & Business Media, 2013.
- [40] J. Eshelby, "Discussion of paper by aj shaler," *Trans. AIME*, vol. 185, no. 11, p. 806, 1949.
- [41] A.-C. Tsai, Y. Liu, X. Yuan, and T. Ma, "Compaction, fusion, and functional activation of three-dimensional human mesenchymal stem cell aggregate," *Tissue Engineering Part A*, vol. 21, no. 9-10, pp. 1705–1719, 2015.
- [42] J. Bico, É. Reyssat, and B. Roman, "Elastocapillarity: When surface tension deforms elastic solids," *Annual Review of Fluid Mechanics*, vol. 50, pp. 629–659, 2018.
- [43] P. Germann, M. Marin-Riera, and J. Sharpe, "ya||a: Gpu-powered spheroid models for mesenchyme and epithelium," *Cell systems*, vol. 8, no. 3, pp. 261–266, 2019.
- [44] E. Palsson and H. G. Othmer, "A model for individual and collective cell movement in dictyostelium discoideum," *Proceedings of the National Academy of Sciences*, vol. 97, no. 19, pp. 10448–10453, 2000.
- [45] J. M. Belmonte, M. H. Swat, and J. A. Glazier, "Filopodial-tension model of convergent-extension of tissues," *PLoS computational biology*, vol. 12, no. 6, p. e1004952, 2016.
- [46] D. J. Durian, "Foam mechanics at the bubble scale," *Physical review letters*, vol. 75, no. 26, p. 4780, 1995.
- [47] B. P. Tighe, "Relaxations and rheology near jamming," *Physical review letters*, vol. 107, no. 15, p. 158303, 2011.
- [48] Y. Mao, A. L. Tournier, A. Hoppe, L. Kester, B. J. Thompson, and N. Tapon, "Differential proliferation rates generate patterns of mechanical tension that orient tissue growth," *The EMBO journal*, vol. 32, no. 21, pp. 2790–2803, 2013.
- [49] S. Okuda, Y. Inoue, M. Eiraku, T. Adachi, and Y. Sasai, "Vertex dynamics simulations of viscosity-dependent deformation during tissue morphogenesis," *Biomechanics and modeling in mechanobiology*, vol. 14, no. 2, pp. 413–425, 2015.
- [50] F. Heinemann, H. Doschke, and M. Radmacher, "Keratocyte lamellipodial protrusion is characterized by a concave force-velocity relation," *Biophysical journal*, vol. 100, no. 6, pp. 1420–1427, 2011.
- [51] E. Ben-Isaac, Y. Park, G. Popescu, F. L. Brown, N. S. Gov, and Y. Shokef, "Effective temperature of red-blood-cell membrane fluctuations," *Physical review letters*, vol. 106, no. 23, p. 238103, 2011.
- [52] J. Ranft, M. Basan, J. Elgeti, J.-F. Joanny, J. Prost, and F. Jülicher, "Fluidization of tissues by cell division and apoptosis," *Proceedings of the National Academy of Sciences*, vol. 107, no. 49, pp. 20863–20868, 2010.
- [53] D. Oriola, R. Alert, and J. Casademunt, "Fluidization and active thinning by molecular kinetics in active gels," *Physical Review Letters*, vol. 118, no. 8, p. 088002, 2017.
- [54] N. I. Petridou, S. Grigolon, G. Salbreux, E. Hannezo, and C.-P. Heisenberg, "Fluidization-mediated tissue spreading by mitotic cell rounding and non-canonical wnt signalling," *Nature cell biology*, vol. 21, no. 2, pp. 169–178, 2019.
- [55] N. J. Balmforth, I. A. Frigaard, and G. Ovarlez, "Yielding to stress: recent developments in viscoplastic fluid mechanics," *Annual Review of Fluid Mechanics*, vol. 46, pp. 121–146, 2014.
- [56] S. Henkes, Y. Fily, and M. C. Marchetti, "Active jamming: Self-propelled soft particles at high density," *Physical Review E*, vol. 84, no. 4, p. 040301, 2011.
- [57] D. Bi, X. Yang, M. C. Marchetti, and M. L. Manning,

- “Motility-driven glass and jamming transitions in biological tissues,” *Physical Review X*, vol. 6, no. 2, p. 021011, 2016.
- [58] S. Kim, M. Pochitaloff, G. Stooke-Vaughan, and O. Campas, “Embryonic tissues as active foams,” *bioRxiv*, 2020.
- [59] M. L. Manning, R. A. Foty, M. S. Steinberg, and E.-M. Schoetz, “Coaction of intercellular adhesion and cortical tension specifies tissue surface tension,” *Proceedings of the National Academy of Sciences*, vol. 107, no. 28, pp. 12517–12522, 2010.
- [60] D. Bi, J. Lopez, J. M. Schwarz, and M. L. Manning, “A density-independent rigidity transition in biological tissues,” *Nature Physics*, vol. 11, no. 12, pp. 1074–1079, 2015.
- [61] M. Merkel and M. L. Manning, “A geometrically controlled rigidity transition in a model for confluent 3d tissues,” *New Journal of Physics*, vol. 20, no. 2, p. 022002, 2018.
- [62] S. Okuda, Y. Inoue, and T. Adachi, “Three-dimensional vertex model for simulating multicellular morphogenesis,” *Biophysics and physicobiology*, vol. 12, pp. 13–20, 2015.
- [63] O. Chaudhuri, J. Cooper-White, P. A. Janmey, D. J. Mooney, and V. B. Shenoy, “Effects of extracellular matrix viscoelasticity on cellular behaviour,” *Nature*, vol. 584, no. 7822, pp. 535–546, 2020.
- [64] C. F. Guimarães, L. Gasperini, A. P. Marques, and R. L. Reis, “The stiffness of living tissues and its implications for tissue engineering,” *Nature Reviews Materials*, pp. 1–20, 2020.
- [65] I. Kosztin, G. Vunjak-Novakovic, and G. Forgacs, “Colloquium: Modeling the dynamics of multicellular systems: Application to tissue engineering,” *Reviews of Modern Physics*, vol. 84, no. 4, p. 1791, 2012.